CrossMark

Nanoparticles of Magnetite in Polymer Matrices: Synthesis and Properties

K. A. Kydralieva[1,3] · G. I. Dzhardimalieva[2,3] · A. A. Yurishcheva[3] ·
S. J. Jorobekova[1]

Abstract This review covers publications on magnetite nanoparticles in polymer matrix, especially in humic acids, which are very interesting, widespread natural polymers. Of special attention was the influence of synthetic conditions on the structure and physicochemical properties of magnetic nanomaterials as well as their potential in environmental applications as sorbents. Nanoparticles of Fe_3O_4 in polymer matrix as promising materials for environmental applications have been in the focus of a great number of studies due to their properties. The modification of magnetic nanoparticles by humic acids leads to increase the sorption properties of such composites and stabilization of magnetite nanoparticles, inhibiting their agglomeration. Thus, humic acids on the one hand, can be used as effective stabilizers for magnetoactive nanoparticles, and on the other hand, keep their protective properties towards ecotoxicants.

✉ K. A. Kydralieva
kamila.kydralieva@gmail.com

1   Institute of Chemistry and Chemical Technology, NAS KR, Bishkek, Kyrgyz Republic

2   Institute of Problems of Chemical Physics, RAS, Moscow District, Chernogolovka, Russia

3   Moscow Aviation Institute, Moscow, Russia

1 Introduction

Currently, particular attention has been given to magnetic nanomaterials owing to the unique properties of magnetic nanoparticles [1, 2] that appeared to be in demand for various applications, e.g., as sorbents for the environmental cleanup of contaminated environments [3–15]. Nanoparticle surface modification by polyfunctional materials with a high sorption capacity is likely to become a mighty tool for control of magnetic characteristics in nanostructures [16, 17].

A concept of functional hybrid nanomaterial design rests on integrating properties of a few materials into the organic whole with a view to afford products with fundamentally new properties. A variety of factors underpins a choice of materials for the fabrication of magnetoactive nanocomposites. To qualify for practical applications such materials should have appropriate functional characteristics and be available. In particular, nanoparticles of ferromagnetic iron, cobalt and nickel outstand with high magnetic moments; nonetheless, they have a few shortcomings such as a propensity for particle surface oxidation by atmospheric oxygen [18] and electric conductivity, which leads to a partial loss of magnetic properties. Iron oxide nanoparticles offer greater opportunities in the preparation of hybrid materials with excellent magnetic performance. Iron oxides are ferrimagnetic compounds whose chief advantages comprise a better adsorption capability and oxidative stability relative to pure iron, which is determinant for sustainability of magnetic properties [18].

This review covers publications on magnetite nanoparticles in polymer matrix, especially in humic acids, which are very interesting, widespread natural polymers. Of special attention was the influence of synthetic conditions on the structure and physicochemical properties of

magnetic nanomaterials as well as their potential in environmental applications as sorbents. Nanoparticles of Fe_3O_4 and γ-Fe_2O_3 as promising materials for environmental applications have been in the focus of a great number of studies [3–15] due to their properties such as well-developed specific surface area [4, 19, 20], colloidal stability [16, 21, 22], and low toxicity [23, 24]. Magnetite surpasses its counterparts (maghemite, ferroxigite) in magnetic properties and, hence, is a prospective candidate as a magnetic inorganic ingredient of hybrid materials. The modification of magnetic nanoparticles by humic acids leads to increase the sorption properties of such composites and stabilization of magnetic nanoparticles, inhibiting their aggregation. Thus, humic acids, on the one hand, can be use as effective stabilizers for nanoparticles, and, on the other hand, keep their protective properties towards ecotoxicants.

2 Physical Characterization of Magnetite

Magnetite pertains to ferrimagnetic compounds, in which an interaction between magnetic moments carried by atoms of sublattices is responsible for the antiparallel orientation; however, common moments in two directions appear dissimilar and the resultant magnetic moment of the substance as a whole is not equal to zero [25].

Magnetite has a face-centered cubic lattice and an inverse spinel structure formed by 32 O^{2-} ions arranged along the direction [111] where one-third of iron (III) cations are distributed across tetrahedral sites and equal amounts of Fe^{3+} and Fe^{2+} ions occupy octahedral positions. Basing on that, the formula of magnetite can be expressed as $(Fe_8^{3+})_t[Fe_8^{3+}Fe_8^{2+}]_oO_{32}$ [26], wherefrom it follows that the ratio of Fe^{2+}:Fe^{3+} = 1:2 in stoichiometric magnetite.

Two different positions of cations in the magnetite structure—tetrahedral occupied by Fe^{3+} ions and octahedral sited by Fe^{3+} and Fe^{2+}—form interpenetrating sublattices with the antiparallel alignment of spins having unequal magnetic moments, what conditions ferrimagnetism. The magnetization is induced by an electron jump between two ions, Fe^{2+} and Fe^{3+}, which coexist in octahedral sites [27]. At that, the specimen is more readily magnetized along the direction [111]. Generally, magnetite is characterized by high magnetic performance, e.g., by data in [26, 28], the coercive force of magnetite particles is 2.4–20 kA/m.

A specific feature of magnetite is chemical instability, with time, resulting in its slow oxidation to ferromagnetic iron (III) oxide under the action of ambient oxygen [19]. Maghemite and magnetite structures can undergo a facile transformation to each other, viz. cautious oxidation of

Fe3O4 gives γ-Fe_2O_3 that converts back to magnetite at heating in vacuo up to 250 °C [26].

3 Methods for Magnetite Nanoparticle Preparation

The classification of nanoparticle preparation methods by a starting substance type and its treatment peculiarities [1] includes two groups of techniques, viz. miniaturization of macroscopic materials (a "up–bottom" approach) and nanoparticle formation by affording a more complex molecular structure through particle assembling from ions, atoms and molecules (a "bottom–up" approach). Both chemical, in the majority of cases based on the "bottom-up" approach, and physical methods are used to prepare magnetite.

According to [29], a chemical process of the magnetite synthesis is comprised of the following basic steps:

(1) preparation of starting solutions;
(2) synthesis of hydroxides; and
(3) formation of magnetite crystal hydrates, from which, subsequently, anhydrous particles of Fe_3O_4 can be isolated by dehydration.

It is possible to suggest a classification of methods for the magnetite synthesis grounded on a feedstock type and the composition of intermediate products (Fig. 1). Nanoscale magnetite can be sourced from e.g., salts of bi- and trivalent iron, taken either combined or individually, bulk magnetite particles and various iron-bearing materials [29]. In most cases, a mixture of Fe^{2+} and Fe^{3+} hydroxides is produced as an intermediate though it exhibits certain particularities and specific properties in each individual synthesis [29].

Chemical methods under the above classification are split to four groups. The first group (options 1–3) includes methods where the feedstock is represented by bivalent iron salt [30–34]. The second comprises processes that employ directly magnetite as the starting material (option 4) [35–37]. To make the chemical classification more comprehensive the proposed scheme [29] has been supplemented by technique 12 based on dissolution of iron-bearing materials [38–40]. Methods that implement the cooperative use of bi- and trivalent iron salts as Fe_3O_4 precursors (options 5–8) fall under the third group [4, 24, 41–52]. Processes where starting compounds are iron (III) salts or oxides are grouped in the fourth pool [5, 27, 53–58].

3.1 Bivalent Iron Oxidation

In case bivalent iron salt is the sole precursor of magnetite, its water solution should be added, apart from alkali, with a
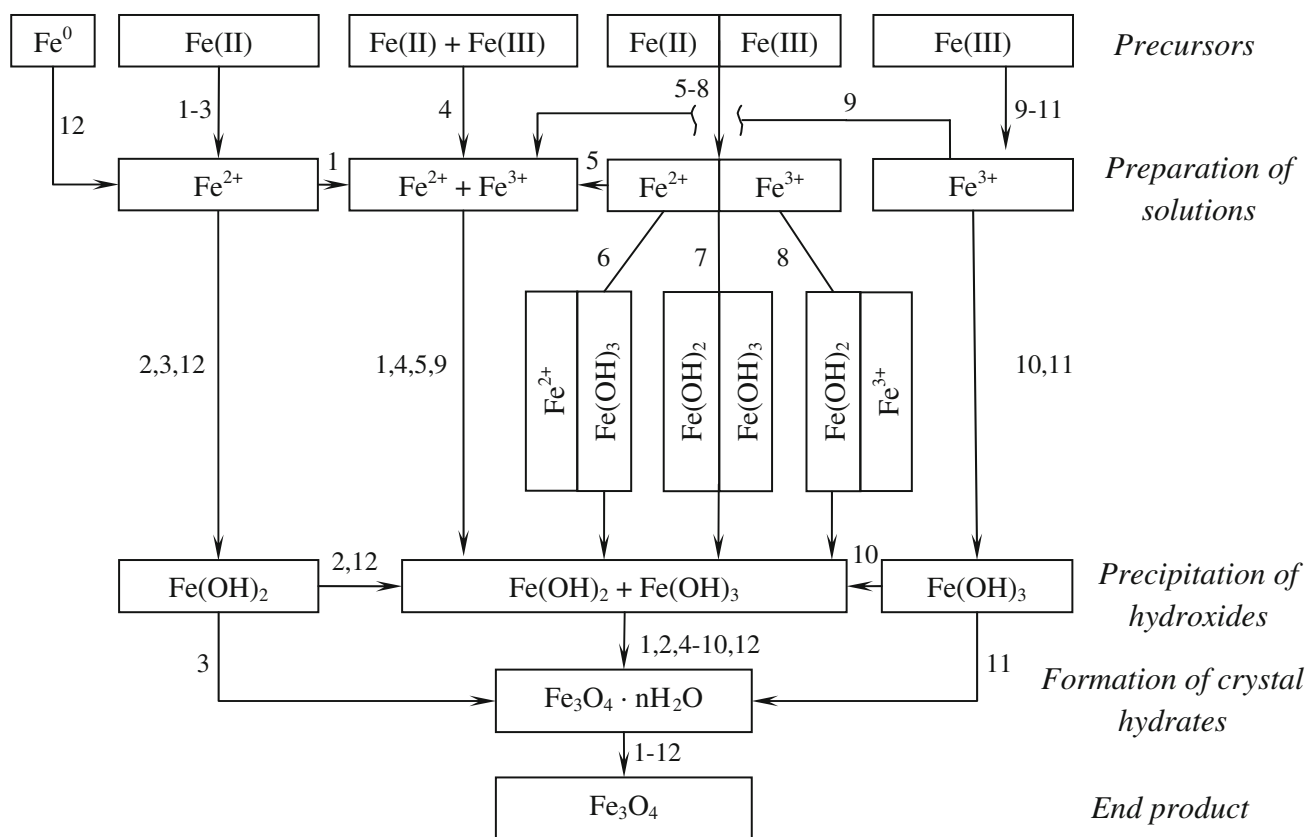
**Fig. 1** Classification of chemical methods for the magnetite synthesis (29 supplemented by technique 12)

measured amount of a weal oxidizer. Here Fe^{3+} ions will be in situ generated since the oxidizer induces a transformation of some part of Fe^{2+} ions to Fe^{3+}. The oxidative hydrolysis reaction described in [30] proceeds in three steps [59]. In the first step, the hydrolysis of bivalent iron salt results in bivalent iron hydroxide:

$$Fe^{2+} + 2OH^- \rightarrow Fe(OH)_2 \qquad (1)$$

Next, a $Fe(OH)_2$ fraction is oxidized to the intermediate, viz. oxyhydroxide of iron (III):

$$3Fe(OH)_2 + \tfrac{1}{2}O_2 \rightarrow Fe(OH)_2 + 2FeOOH + H_2O \qquad (2)$$
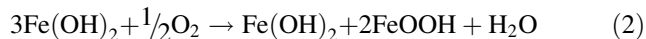
The final step yields magnetite via a dehydration reaction between iron (II) hydroxide and iron (III) oxyhydroxide:

$$Fe(OH)_2 + 2FeOOH \rightarrow Fe_3O_4 + 2H_2O \qquad (3)$$
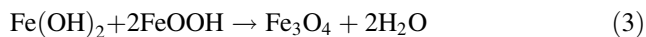
In the study [31], 30–100 nm magnetite particles were prepared at different temperatures in the high alkaline medium (NaOH, pH = 12–13) with the addition of $NaNO_3$ as an oxidizer. A temperature increase from 4 to 37 °C involved a decrease in the particle size from 102 ± 5.6 to 31.7 nm and the particle shape was changing from octahedral to actually spherical. However, of note is that control of the magnetite generation as the pure phase was

hampered in this group of methods because oxidation of Fe^{2+} is a kinetically decelerated process.

3.2 Dissolution of Iron-Bearing Materials

An example of the magnetite particle synthesis under the second group of methods is chemical dissolution of bulk magnetite followed by precipitation. In the research [35], a natural magnetite specimen was milled to 0.02–0.04 mm particles in inert nitrogen or carbon dioxide media with a view to accelerate magnetite dissolution in an inorganic acid (hydrochloric, sulfuric or orthophosphoric). The Fe^{3+}/Fe^{2+} ratio in the solution prepared in this manner was 2:1 just as in stoichiometric magnetite. Upon the introduction of excess alkali (NH_4-OH, NaOH or KOH) to the solution of iron salts, the precipitate, at a few minutes, converts to magnetite crystal hydrates. Anyhow, this process is rather labor-intensive and, where starting magnetite bears impurities, it calls for extra synthetic steps since there appears a need for adding aqueous solutions of bi- and trivalent iron in order to adjust the Fe^{3+}/Fe^{2+} ratio.

Also, another method to prepare magnetite using anodic dissolution of iron-bearing materials is known [39]. The main benefits of this process are pure end products and

control of their dispersity by monitoring of electric parameters of the electrolysis.

The concept of the method reported in [39] draws on anodic dissolution of carbon steel St3 in a sodium chloride solution and oxidation of intermediates by oxygen of applied air; herein the key process on the anode was iron dissolution:

$$Fe^0 \rightarrow Fe^{2+} + 2\bar{e}, \tag{4}$$

meanwhile hydrogen emission occurred on the cathode involving solution alkalization:

$$2H_2O + 2\bar{e} \rightarrow H_2 + 2OH^- \tag{5}$$

The anode and cathode reaction products interacted and yielded iron (II) hydroxide which was partially oxidized by ambient oxygen:

$$Fe^{2+} + 2OH^- \rightarrow Fe(OH)_2 \tag{6}$$

$$2Fe(OH)_2 + H_2O + {}^1\!/_2 O_2 \rightarrow 2Fe(OH)_3 \tag{7}$$
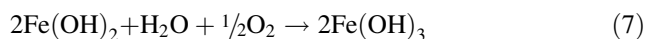
The resulting bi- and trivalent iron hydroxides reacted to give dispersed magnetite with particles sized below 40 nm [39]:

$$2Fe(OH)_3 + Fe(OH)_2 \rightarrow Fe_3O_4 + 4H_2O \tag{8}$$
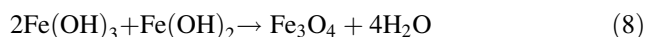
The properties of the prepared particles were shown to be affected by the parameters such as the current density, sodium chloride solution concentration and temperature as well as by pH of the medium [39]. These parameters varying allows for control of the end product properties. However, a shortcoming of the method is its rather low productivity.

3.3 Reduction of Iron (III) to Iron (II)

Of knowledge are magnetite preparation methods where Fe^{3+} irons serve as iron oxide precursors. For instance in [53], magnetite nanoparticles were synthesized by boiling of a solution of iron (III) chloride crystal hydrate ($FeCl_3 \cdot 6H_2O$) in 2-pyrrolidone for 1, 10 and 24 h in nitrogen atmosphere. Their generation mechanism includes interrelated processes of pyrrolidone-2 decarbonylation and a reductive hydrolysis of iron chloride to Fe_3O_4.
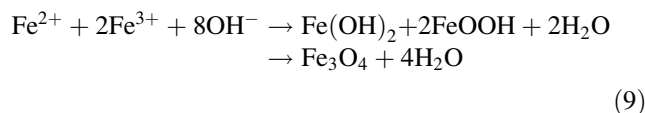
Among the magnetite synthesis techniques is thermal decomposition of Fe^{3+}—containing compounds where Fe^{3+} undergoes partial reduction to Fe^{2+} at high temperatures (100–370 °C) and with scarce oxygen. Magnetite particles 5–8 nm in size are formed under thermal destruction of $Fe(acac)_3$ in diphenyl ether in the presence of hexadecane-1,2-diol [54]. The paper [55] communicates a magnetite synthesis by thermal decomposition of iron oxalate $Fe_2(C_2O_4)_3 \cdot 5H_2O$ at 375 °C. Thermal decomposition is an efficient method to prepare iron oxide

nanoparticles that exhibit high stability in solution, which enables control of the particle size and morphology [27]. Nevertheless, the method has a shortcoming such as a hydrophobic coating present on the surface of nanoparticles and, hence, requires additional modification for achieving solubility in the aqueous medium [60]. Moreover, high cost of the feedstock and sophisticated processes of iron (III) reduction constrain extensive applicability of the method, for the exception of cases where trivalent iron salt or oxide is sourced from industrial waste.

3.4 Coprecipitation of Bi- and Trivalent Iron Salts

The most widespread methods of the nanomagnetite formation are those based on the cooperative use of Fe^{3+} and Fe^{2+} salts [1]. They allow the fabrication of Fe_3O_4 particles with adjustable sizes, which becomes feasible by varying synthetic conditions. In this context, the methods show promise in developing Fe_3O_4 nanoparticles with preset characteristics.

Chemical coprecipitation of bi- and trivalent iron salts stands among the most facile synthetic pathways because it suggests a one-step preparation of high magnetite amounts. Generally, the synthesis of Fe_3O_4 by coprecipitation of Fe^{3+} and Fe^{2+} salts can be presented as the reaction:

$$\begin{aligned} Fe^{2+} + 2Fe^{3+} + 8OH^- &\rightarrow Fe(OH)_2 + 2FeOOH + 2H_2O \\ &\rightarrow Fe_3O_4 + 4H_2O \end{aligned} \tag{9}$$

The end product morphology depends on a type of salts utilized as precursors (nitrates, sulfates, and chlorides), precursors' molar ratio, reaction medium temperature, pH, and the ionic interaction force of the medium [61, 62]. Operational parameters of the rational magnetite synthesis process using coprecipitation of bi- and trivalent iron salts can be expounded as follows:

– *iron chlorides* are the best applicable precursors for the magnetite synthesis because of their high hydrolysis ability and a lack of impact on hydroxy complexing;
– *a ratio of bi- and trivalent iron salts* in chemical coprecipitation has to be *1:2* since a deviation from the stoichiometric composition can adversely influence the end product properties [1]. Nevertheless, there are researches [63, 64] where Fe_3O_4 nanoparticles were synthesized at a $Fe^{2+}:Fe^{3+}$ ratio different from the stoichiometric;
– the optimal *pH value* in the magnetite synthesis lies in the *range of 7–8* as these are the values, at which cations of iron (III) exist in the active form. Magnetite may be regarded as the product of the interaction between a weak base of iron (II) hydroxide and a weak "ferric" acid $Fe(OH)_3$ [65]. To afford Fe_3O_4 the

reaction medium has to be neither superfluously alkaline nor acidic—in this sole case hydroxides are able to exhibit their basic and acidic properties and react with each other in a proper way. Both hydroxides in the strongly alkaline medium behave as weak acids, i.e., dissociate to split off the hydrogen ion, which fails to result in magnetite [65]. Given that optimal solution pH is the one, at which the formation of hydroxides by the hydrolysis of iron salts proceeds and at the same time the basic properties of iron (II) hydroxide are not suppressed. Apart from that, the availability buffer properties with the alkaline solution is crucial: in this event, the pH value does not undergo substantial changes in the course of salt solution mixing with alkali and under the hydrolysis [65]. *Hydrous ammonia* is most suitable for maintaining these conditions;

– a synthesis temperature increase involves a reaction rate buildup; maximum product yield is achievable in the *30–40 °C temperature range* [66].

As shown in the study [67, 68] by X-ray diffraction analysis, the key component of the powder synthesized in the above-described synthetic conditions was magnetite Fe_3O_4 (Fig. 2), which was evidenced by interplanar distances d and distribution of intensities I of diffraction fringes.

The average particle size determined by the Scherrer equation was 9.2 nm.

According to electron micrographs (Fig. 3), the native magnetite structure was presented in the form of associates comprised of magnetite nanoparticles.

Isostructurality of magnetite and maghemite characteristic of a cubic lattice, spinel pattern and close values of crystal lattice parameters makes it difficult to unambiguously identify diffractograms that correspond to magnetic powder particles. For more accurate identification of the
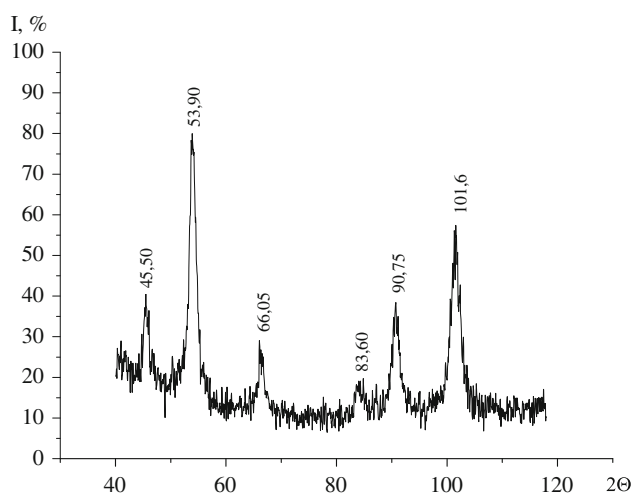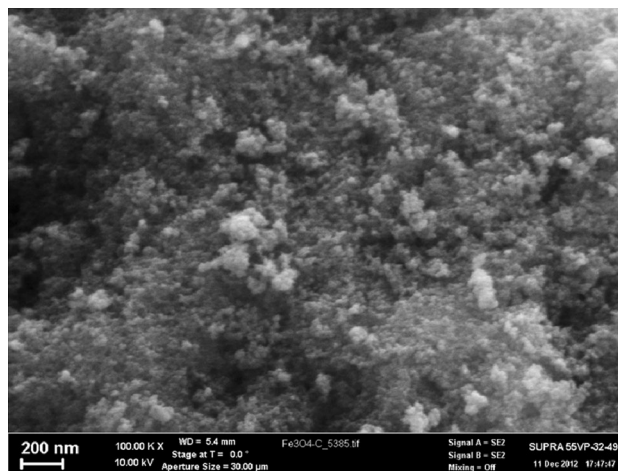

Fig. 3 SEM micrographs of magnetite

phase composition, the iron oxide structure was analyzed by Mössbauer spectroscopy at 5 K̇ (Fig. 4) [69]. It showed that the structure was a well-resolved sextet of five nonequivalent sites of iron atoms: two sites corresponded to trivalent iron atoms in the tetrahedral and octahedral surroundings, and the other three were assigned to bivalent iron atoms in the octahedral surrounding, which fits the structural formula of magnetite [26].

Pathways of generating nanoparticles either in gas or in solid phase assisted by high energy impacts on the material are commonly referred as physical methods [1]. Researches dealing with the magnetite preparation by these techniques are rather scarce and reduced to condensation from oversaturated metal vapors and dispersion of the compact material.

The classical nucleation theory that describes new-phase nucleating clusters by a spherical drop model underpins a route of the nanoparticle preparation by precipitation from the gas phase [1]. Various metal evaporation techniques are utilized to prepare nanoparticles, e.g., the authors of [21] suggested heating of a mixture of Fe_3O_4 gaseous precursors by a laser beam in the gas mix flow that resulted in 5–7 nm nanoparticles with narrow distribution.
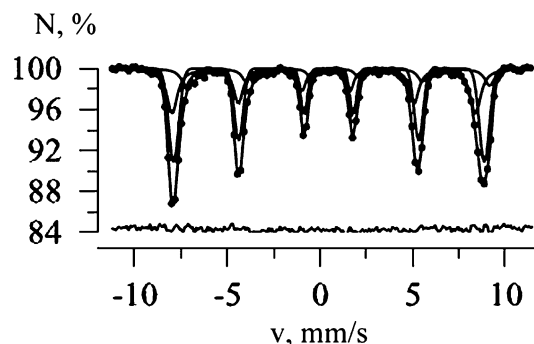

Fig. 2 Diffractogram of magnetite

Fig. 4 Mössbauer spectra of magnetite recorded at 5 K̇ [67]

As for the dispersion routes, most widespread is a method of mechanical material activation in mills of different design. These studies rest on two principles, viz. intermittent nature of the process (the alternation of relaxation and stress field formation) and local nature of mechanical impact on a substance (a stress field is induced at the solid particle contact with another particle or a working medium) [70]. Mechanical activation of a powder is performed for providing the energy accumulation in the form of flaws or other modifications in the substance in order to reduce activation energy of its chemical transformation or to improve the steric condition of the process [70].

Two mechanical activation types are distinguished [70]:

(1)   mechanical activation reactions where the time of mechanical impact and stress field formation and its relaxation exceeds the chemical reaction time; and

(2)   mechanical activation as such where the mechanical impact and stress field formation time is less than the chemical reaction time or these processes are time-spaced.

A sequence of the processes occurring under mechanical activation of solids can be conditionally split to the stages: reagent dispersion—mechanical mixing—chemical interaction.

Of knowledge are various procedures to prepare magnetite by mechanical activation [67, 71–74]. For instance, aqueous suspensions of ferric hydroxide at pH values between 2.9 and 13.3 were used as the starting material and milled in a stainless steel horizontal tumbling ball mill; although the milling was performed without heating and in the absence of any reducing agent, magnetite nanoparticles with a diameter of 10–20 nm were formed [72].

A mechanochemical synthesis was applied to afford magnetite nanoparticles from salt systems [73]. Here a chemical reaction proceeded on interphase surfaces that continuously regenerated under ongoing iron chlorides activation and dispersion in the presence of sodium chloride. To prepare different size of particles, the as-milled powders were annealed at temperatures ranging from 100 to 800 °C for 1 h in 10 % H_2/Ar mixed gas. The average crystallite size of the powders varied from 12.5 to 46 nm by changing the annealed temperatures and the corresponding saturation magnetization value ranged from 52 to 66.4 emu/g [73].

Since the densely-packed oxygen lattice of spinel is retained under mechanical activation and main changes occur in the cationic lattice, which are expressed in redistribution of bi- and trivalent cations in octa- and tetrahedral voids [70], dispersion of spinel-structured iron oxides can be viewed as a prospective research area. For example, a method of preparing spinel Fe_3O_4 by mechanical treatment

of hematite α-Fe_2O_3 with mean particle size 30 nm was reported in [74].

Comparative data on nanoscale magnetite preparation methods are summarized in Table 1.

4 Stabilization of Magnetite Nanoparticles

Nanoscale magnetite particles have a propensity for aggregation owing to high surface energy inherent in finely-divided structures. Colloidal electrostatic stabilization is normally insufficient for preventing the aggregation in solutions because of a higher force of magnetic interactions between particles [27]. To this end, it is impossible to separate nanoparticle generation and stabilization methods [1]. On the surface of each particle there always are its chemical modification products which significantly influence the nanomaterial properties [1]. It is especially important for magnetic nanoparticles whose modified surface layer may have magnetic characteristics absolutely different from those of the particle nucleus [49, 76]. Thus, oxidation of iron (II) oxide can occur in the particle's surface layer incorporated in magnetite, which involves a decrease in saturation magnetization [76].

Figure 5 demonstrates the different structures; among them the two types of core–shell structure (cores with organic and inorganic shell) in two categories (grafted magnetic nanoparticles with a polymer coating and core/shell nanoparticles) and heterodimer nanostructures. According to a recent review [77], the literature distinguishes in situ coating, post-synthesis adsorption or post-synthesis grafting [78] onto magnetic nanoparticles.

The most extensively used methods of magnetic nanoparticle stabilization are the immobilization in the polymer matrix and the formation of core/shell structures (Fig. 6) that enable limiting the particle size growth due to the encapsulation inside of the stabilizer matrix [79].

Core/shell structures can be attained using silicon oxide or gold for encapsulating magnetic nanoparticles. These inert coatings protect the magnetic core from chemical degradation. Silicon oxide shells are also frequently utilized as a protective coating for magnetic nanoparticles owing to their stability in the aqueous medium and facile synthesis [6, 80–82].

The size and colloid stability of iron oxide particles can be notably affected by chelating organic anions (carboxylate ions such as citric, gluconic or oleic acids) or polymers (dextran, starch, polyvinyl alcohol, polyethylene glycol, polyvinyl ethanol, heparin, humic acids, and pectin) introduced to the reaction medium in the ongoing nanoparticle formation [67, 83–85] or post-coating of magnetic nanoparticles [86–88].

Table 1 Methods for the preparation of magnetite nanoparticles [data sourced from 65, 75] and their characterization

| Preparation method	Nanoparticles characteristics						
	Size		Shape control	Synthesis	Reaction		
	Range (nm)	Distribution			Temperature	Time	Yield
Aerosol pyrolysis	5–60	Broad	High	Complicated, vacuum/controlled atmosphere	High/very high	Minutes/hours	Medium
Gas deposition	5–50	Narrow	High	Complicated, vacuum/controlled atmosphere	Very high	Minutes	High
Sol–gel	3–150	Narrow/broad	High	Simple	20–90 °C	Hours/days	Medium
Co-precipitation	10–50	Broad/narrow	Medium	Very simple	20–90 °C	Minutes	High
Thermal decomposition	2–20	Very narrow	Very high	Complicated, inert atmosphere	100–330 °C	Hours	High
Microemulsion	4–15	Narrow	High	Complicated	20–70 °C	Hours/days	Low
Electrolytic condensation	30–80	Narrow/broad	Medium	Complicated	20–90 °C	Hours	Low
Hydrothermal	10–150	Narrow	Very high	Simple, high pressure	100 °C–high	Hours/days	Medium
Mechanochemical synthesis	30–500	Broad	Medium	Very simple	20 °C	Minutes/hours	High
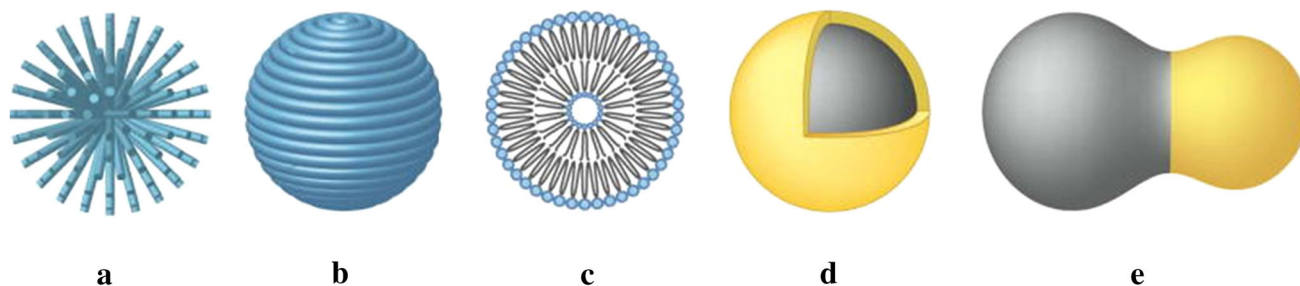
Fig. 5 Magnetite nanoparticle structures and functionalization schemes: **a** grafted magnetic nanoparticles with a polymer coating; **b** nanoparticles encapsulated in the polymer matrix; **c** nanoparticles encapsulated in liposomes; **d** core/shell nanoparticles; **e** heterodimer nanostructures [27]

Fig. 6 Core/shell structure of metal-polymer nanocomposite $Fe_3C(FeAAm)$

Polymer shell

M_xO_y, M_xC_y -shell

M_x-core

Polymer matrix
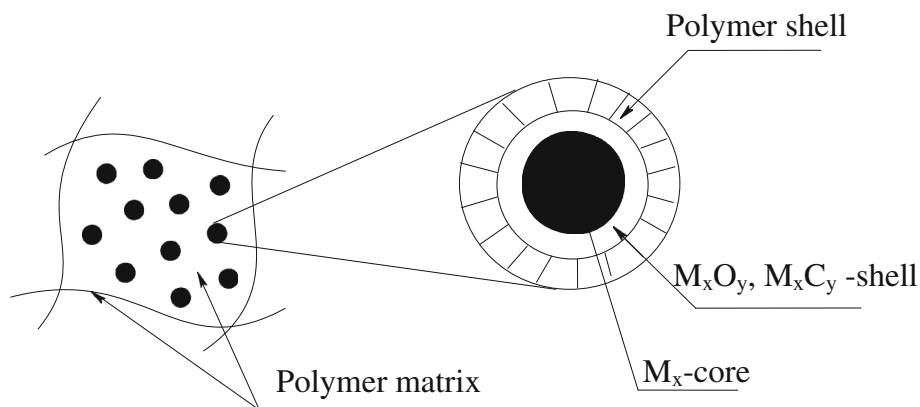
In so doing, apart from nanoparticle size diminishing relative to native magnetite, a narrowing of their values scatter was marked [89].

An interaction between carboxyl groups of polyacrylic acid and magnetite nanoparticles was described in the paper [90]. As one macromolecular chain of polyacrylic acid can react with more than one particle capable of simultaneous binding with functional groups of different macromolecules, conditions for the formation of cross-linked structures were created (Fig. 7).

Polymer macromolecules coordinate and hold iron ions and growing particles in the interchain space thereby efficiently stabilizing the latter and regulating their size. Functional moieties (macromolecules with electron-donating groups, such as hydroxyl and carboxyl ones, presiding) or heteroatoms capable of coordination, which are present in the polymer, facilitate a better targeted and more intensive interaction. Polymer chains and nanoscale voids representing a vacant volume between polymer's macromolecules vigorously affect nanoparticles being formed through control of their characteristics such as the growth, size, and chemical surrounding of inorganic phase [16]. In turn, growing seeds having gained a nanometer size build in the polymer matrix driven by high surface energy.

Much interest has been recently attached to processes that comprise in situ stabilization of nanoparticles by polymers [91]. The processes have a number of advantages over stepwise modification of nanoparticles, including aggregation reduction due to particles coating directly in the nucleation step and a decreased number of treatment steps. However, the involvement of polymers in the nucleation and growth of nanocrystals is likely to dramatically influence the nanoparticle crystal structure and morphology. Findings in [92] evidence that crystallinity decreases as the
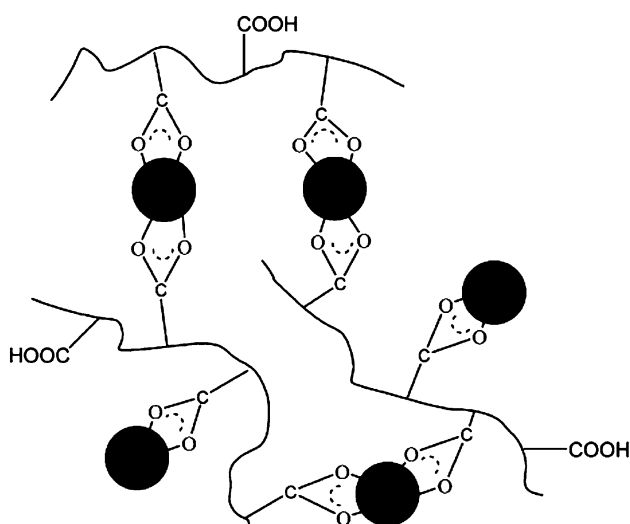
concentration of polyvinyl alcohol, which is present in the magnetite synthesis reaction medium, increases. Given that, in polymeric coating applications, it is necessary to make allowance for the structural imperfection of nanoparticles that can cause lower magnetic properties [27].

Core/shell structures were attained by UV-initiated polymerization after the addition of a 2-hydroxyethylmethacrylate solution and a cross-linker N,N′-methylenebisacrylamide to the washed and ultrasound-irradiated magnetite nanoparticles (14 ± 1 nm) [93]. A gel shell was formed on the nanoparticle surface as a result of copolymerization of vinyl groups of starting compounds. It was possible to change the size of magnetic gel particles by varying the monomer volume or the irradiation time [93].

Therefore, a material with the preset composition and morphology can be synthesized by combining precursors with account for their chemical nature, by varying component concentrations, and by selecting synthetic conditions such as temperature and pH. Of special attention in the hybrid material preparation is the nature of interphase interactions that can be governed by van der Waals forces, hydrogen bonds, hydrophilic and hydrophobic interactions, and by covalent or ionic bonds. The emerging interactions and bonds between polymeric organic macromolecules and inorganic nanostructures are determining for a set of properties of organic–inorganic hybrid materials.

5 Functional Properties of Magnetite-Based Composite Materials

Hybrid materials based on nanoparticles of iron oxides and polymers can be regarded as polymer matrices with high-dispersive magnetized particle inclusions [18]. Designing of such composites conceptually builds on the integration of properties of an organic material and of inorganic nanoparticles.

By using various techniques, it is possible to synthesize materials with preset morphology and a requisite amount of the magnetic constituent. The composites potentially have a wide scope of applications—from the magnetic separation of versatile technical media to the preparation of polymeric suspensions for biomedicine [18, 94].

5.1 Magnetic Properties

Magnetic characteristics of nanocomposites bearing magnetite particles depend both on interactions between particles of the magnetic nanophase and on the particles size of the magnetic component: at its reduction below a certain critical value (30 nm for magnetite [26]), the domain structure is no longer advantageous in terms of energy and particles acquire a single-domain structure. A system of the

Fig. 7 Cross-linked gel structure on the basis of polyacrylic acid and Fe$_3$O$_4$ [90]

single-domain nanoparticles assumes new magnetic properties, i.e., transfers to a superparamagnetic state. The superparamagnetic particles behave in the same manner as paramagnetic ones though they have a much higher magnetic moment: residual magnetization is lacking, the coercive force is zero, and they do not have the hysteresis loop depending on the magnetization intensity from the external magnetic field [18].

A mechanism of the particle size influence on magnetic characteristics has not been ultimately elucidated. The study [95] communicates a saturation magnetization drop alongside with particle size reduction. It was 84 emu/g for particles with the average size 40 nm, 82 emu/g for particles 35 nm in diameter, and 76 emu/g for particles 22 nm in diameter.

The authors of [96] observed a weakening of magnetic properties with particle size reduction, viz. 85 emu/g for 17 nm particles and 78 emu/g for particles with the average diameter 5 nm. The coercive force also came down with a particle size decrease, viz. 400 Oe for 17 nm particles and 250 Oe for particles with the average diameter on the order of 5 nm.

Magnetic characteristics depend on a stabilizer and a nanoparticle generation method. For example, oleic acid taken as a stabilizer led to a weaker interparticle dipole interaction [96]: the coercive force for particles of native or oleic acid-coated magnetite was 500 and 250 Oe, respectively.

In the study [97], magnetite nanoparticles were synthesized by two methods—chemical coprecipitation and thermal decomposition. Here saturation magnetization and the coercive force of magnetite nanoparticles were 46 emu/g and 500 Oe under chemical coprecipitation and 84 emu/g and 400 Oe under thermal decomposition.

In case of low concentration of nanoparticles in the matrix, nanocomposites are superparamagnetic, due to the directions of weak magnetization axes, which are distributed randomly. High concentration of nanoparticles in the matrix results to a reaction between them, that form infinite conductive cluster, and the nanocomposite exhibit ferromagnetic properties [98]. The magnetization of the samples of polyvinylidene fluoride (PVDF) with Fe_3O_4 and polyethylene (PE) with Fe_3O_4 has superparamagnetic character. Specific magnetization for nanocomposite on the basis PVDF is higher than the one for PE basis. Magnetic perception depends on supermolecular structure of polymer and crystallization degree. Change of specific magnetization depending on magnetic field and polymeric matrix type can be link with difference of diamagnetic anisotropy, supermolecular structure and crystallization degree of polymeric matrix PVDF and PE [98].

It is established experimentally that specific magnetization of Fe_3O_4 nanoparticle in the polymer also depends on temperature-duration regime of polymer crystallization. The value of specific magnetization of $PE+Fe_3O_4$ changes depending on temperature-duration regime of polyethylene crystallization, it means specific magnetization of $PE+Fe_3O_4$ increases with declining of temperature-duration regime of polyethylene crystallization [98].

Summing up, the structural characteristics change enables control of magnetic interactions between nanocomposite particles underlying magnetic properties of the material on the whole.

5.2 Sorption Potential in Regards to Ecotoxicants

Limited research on application of magnetite nanoparticles in the environmental area are reported [3–15, 89, 99–102]. While magnetite and maghemite nanoparticles were applied to the removal of Cr(VI), chitosan-bound Fe_3O_4 magnetic nanoparticles were prepared for the removal of Cu(II) ions [101]. Brief review on the application of magnetic nano- and microparticles in the removal of metals in wastewaters was given in [99].

Self-assembled 3D flowerlike iron oxide nanostructure materials were demonstrated to have an excellent ability for the removal of As(V), Cr(VI), and Orange II from water [5]. Nanocrystals of monodisperse Fe_3O_4 were exploited to remove arsenic from water with magnetic separations at very low magnetic field gradients [89]. The removal efficiency of As(III) and As(V) increased by orders of magnitude by reducing the diameter of Fe_3O_4 nanocrystals from 300 to 12 nm. The Fe_3O_4 composite with dimercaptosuccinic acid was used for the removal of Hg, Ag, Pb, Cd, and Tl [102]. Bare magnetite nanoparticles are very much susceptible to air oxidation [103] and are easily aggregated in aqueous systems. Some samples of magnetite sorption ability of different types of contaminants are summarized in Table 2.

Thus, synthetically prepared magnetite is a potential agent for remediation of polluted water [76, 103]. Colloidal instability and tendency to aggregate is reduced and/or eliminated by modifying of the nanoparticles surface. The modification of magnetic nanoparticles by polyfunctional organic substances leads to increase the sorption properties of such composites. The advantage of these materials compared with traditional sorbents is the ability to extract them from the solution after sorption using magnetic field [55]. From this standpoint, humic acids (HA) are natural macromolecular polyfunctional ligands with high exchange capacity (4.7–14.2 meq/g), are promising candidates.

6 Magnetite Nanoparticles in Humic Matrices

Humic acids constitute an organic macrocomponent of soil and water ecosystems as well as of solid fossil fuels. They account for 60–80 % of the organic matter total in soil and water and vary from 20 to 90 % in peat and coal [110, 111].

Table 2 Adsorption of magnetite composites towards different types of pollutants

Sorbent	Contaminant	Max. adsorption capacity (mg/g)	Conditions	Size of magnetite nanoparticles (nm)	Saturation magnetization (emu/g)	Reference
Magnetite/sepiolite composite	Co(II)	18.85	293 K	–	16.85	[14]
	Cd(II)	14.15				
Graphene oxide–magnetitehybrid	Sr(II), Co(II)	–	pH > 5	15–21	31	[104]
Magnetite nanospheres	Cr(II)	9	pH 4.0	30–45	77.5	[105]
	Pb(II)	19	pH 5.0			
Corn cob activated carbon coated with nano-sized magnetite particles	Cr(VI)	57.37	pH 2	50	48.43	[106]
3-Mercapto-propionic acid functionalized magnetite nanoparticles	Ni(II)	42.01	pH 6.0, 303 K	11–18	14.02	[107]
Cetyltrimethyl-ammonium bromide-coated magnetite nanoparticles	Reactive black 5 (RBBA)	312.5	–	20	76	[108]
	Reactive red 198 (RRR)	163.9				
	Reactive blue 21 (RTB)	556.2				
Magnetite nanoparticles coated with a poly(γ-glutamic acid)	Methylene blue dye	78.67	within 5 min	12.4	59.2	[109]
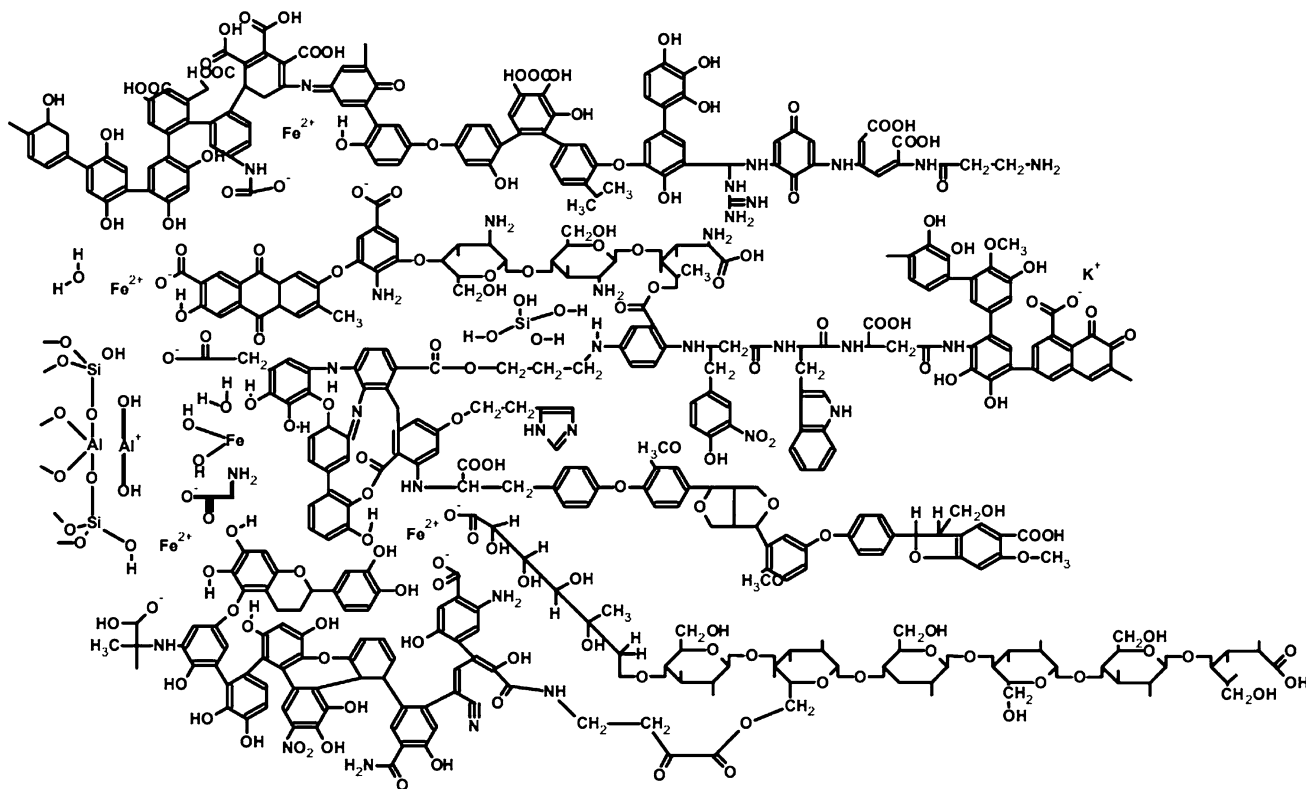
Fig. 8 Hypothetic structural fragment of humic acids [112]

A hypothetic structural formula of the HA fragment in soils suggested by Kleinhempel is presented in Fig. 8 [112]. The formula comprehensively depicts both the stoichiometric nature of the HA structure and a set of possible incorporated structural fragments.

From various data sources, the HA molecular mass is known to range over 700–200,000 D.

It is of common knowledge that an HA macromolecule consists of the "backbone" and periphery [113]. The backbone is comprised of heavily substituted aromatic moieties bonded by alkyl, ether, etc. bridges.

The carbon distribution across structural fragments, determined by ^{13}C NMR spectroscopic integration (Fig. 9) over six spectral ranges where groups of carbon atom signals with a similar chemical environment are located, is indicative of a high aromatic carbon content, viz. above 50 %, and an actually zero carbohydrate periphery (CalkO concentration below 10 %) (Table 3).

Predominating substituents are oxygen-containing functional groups, namely carboxyl, phenolic and alcoholic hydroxyl, carbonyl and methoxy groups [113]. The periphery is represented by a carbohydrate-protein complex covalently linked to the backbone. Additionally, the periphery includes ash constituents such as silicates, aluminosilicates, iron oxides, etc. linked to the organic matrix by oxygen bridges [113].

Owing to the unique structure that incorporates the aromatic core heavily substituted with various functional groups and the hydrophilic carbohydrate periphery, humic acids are able to enter into almost any type of interactions (Table 4), especially to the formation of strong complexes of humic acid with metal ions [114–118].

Thus, the important protective function of HA involving their ability to bind inorganic and organic ecotoxicants in polluted and soil environments into the strong complexes is performed [117]. The complexation reactions of macromolecular ligands with metal ions are also of practical importance due to the possibility of their use in the concentration and separation of trace amounts of metals. The prospects of practical use of HA and their derivatives as environmentally safe natural sorbents are determined by huge resources of humus-containing raw materials including brown coal, peat, sapropel, etc.

Electron micrographs of HA samples show that humic acids are loose non-homogenous associates with a well-developed porous structure, i.e., globules formed by hydrogen bonds and chemical forces. In general, such HA associate is penetrable by iron oxide molecules and iron ions and underlies a bulky nature of ion exchange and iron oxide molecule binding processes. This structure of HA molecules and large-volume sorption prevent the generation of the monomolecular layer from sorbed HA molecules on the Fe_3O_4 surface; the discrete arrangement of active sites provided by electrostatic bonds of iron ions with reactive HA groups in the HA macromolecule volume should be regarded as well-substantiated in terms of physics.

Findings in [4, 42, 43, 50] evidence that humic acids efficiently stabilize magnetite nanoparticles. Humic acids have a high affinity to Fe_3O_4 nanoparticles, and sorption of HA on the Fe_3O_4 nanoparticles enhance the stability of nanodispersions by preventing their aggregation [87, 88].

Recent research indicated that humic acid-coated manganese ferrite ($MnFe_2O_4$/HA) magnetic composite materials prepared with chemical coprecipitation method. The results show that the size of the product is about 200 nm. $MnFe_2O_4$/HA has a typical spinel structure and is successfully coated with humic acid on its surface. The

Fig. 9 ^{13}C NMR spectra of the HA sample (the spectra were recorded on a Bruker Aspect 3000, frequency 100 MHz at 303 Қ, time delay between pulses—8 s, 5 mm sensor, solvent—0.3 M NaOD, sample weight—50–70 mg)
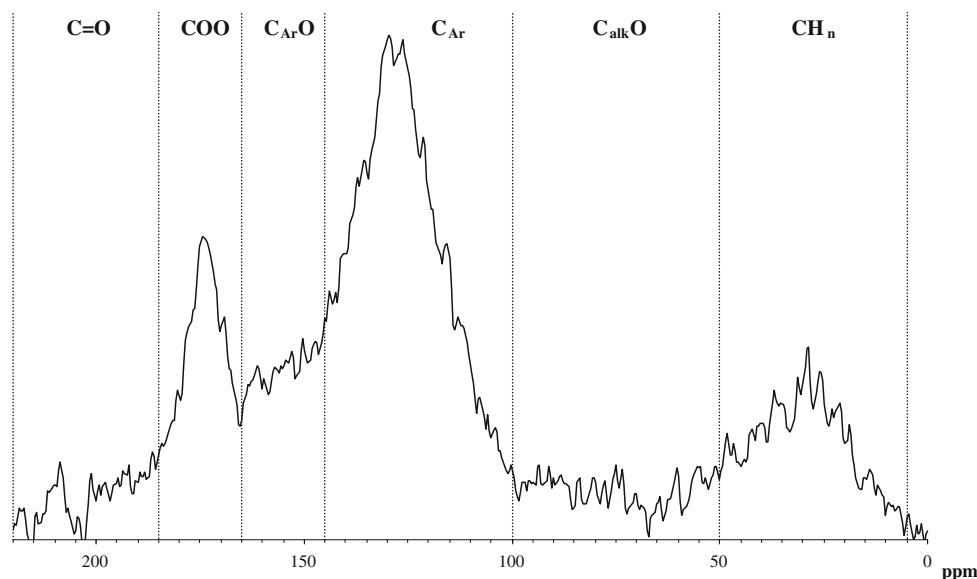
Table 3 Carbon distribution by structural fragments (in % of the carbon total) in humic acids

C=O	COO	CarO	Car	CalkO	CHn	$\sum$Car	$\sum$Calk
5.4	13.1	11.8	47.1	9.2	15.4	52.2	29.4

$\sum$*Car* aromatic carbon total (CarO + Car), $\sum$*Calk* aliphatic carbon total (CalkO + CHn)

Table 4 Main structural HA fragments responsible for mechanisms of binding with ecotoxicants [117]
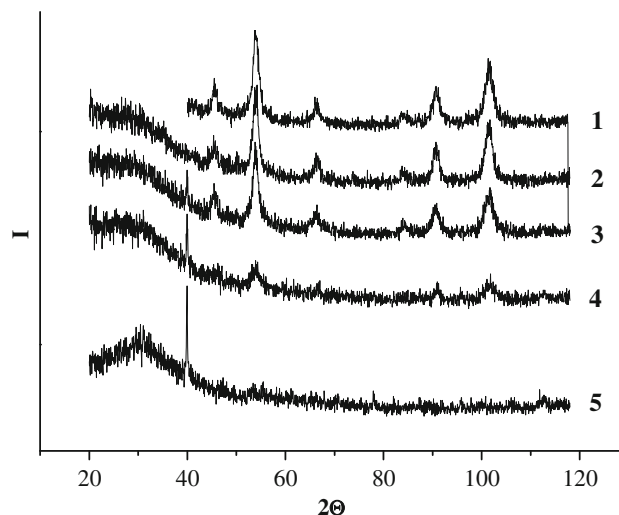
Structural fragment	Interaction type
–COOH	Ion exchange
–OH	Donor–acceptor interaction
>C=O	(Complexing with a charge transfer, hydrogen bonds, etc.)
[benzene ring structure]	Van der Waals bonding, incl. hydrophilic bonds
–CHn–	

Fig. 10 X-ray diffraction analysis data for hybrid materials synthesized by in situ chemical coprecipitation: *1* Fe_3O_4, *2* Fe_3O_4-HA20-C, *3* Fe_3O_4-HA50-C, *4* Fe_3O_4-HA80-C, *5* HA (index "C" means coprecipitation, number index—concentration of HA in wt%)

saturation magnetization of $MnFe_2O_4$/HA is 34.01 A m^2/kg. $MnFe_2O_4$/HA can be separated from water with low magnetic field within 30 s. The adsorption of methylene blue is a pseudo second-rate kinetic process and reaches equilibrium in about 2 h, in good agreement with the Langmuir adsorption model. $MnFe_2O_4$/HA has higher adsorption ability than that of pure $MnFe_2O_4$. The max adsorbing capacity can reach 29.94 mg/g at room temperature and pH = 9. $MnFe_2O_4$/HA can be used as adsorption material for effective removal of methylene blue from waste water [119].

Parallel generation of other iron oxide species was reported in [50, 68]. The authors carried out a comparative analysis of two pathways of forming magnetic nanoparticles—solid phase synthesis in a high-energy ball mill and chemical coprecipitation (in situ) in the HA matrix. They showed that the HA addition did not distort the diffraction pattern characteristic of Fe_3O_4 nanoparticles (Fig. 10). By XRD analysis, the major magnetoactive component for materials prepared by dissolution in argon was magnetite Fe_3O_4. Herewith, the intensity of magnetite peaks reduced as the HA concentration in hybrid materials was growing. Average particle sizes calculated by the Scherrer equation tended to decrease from 8.4 nm for Fe_3O_4/HA20-C to 4.5 nm for Fe_3O_4/HA80-C.

The diffractograms of the nanoscale magnetite samples prepared by the mechanochemical method in the HA presence displayed additional peaks uncharacteristic of the magnetite phase.

The Mössbauer spectra of hybrid materials produced from magnetite and HA by chemical coprecipitation in argon were typical for superparamagnetic particles (Fig. 11). A quadrupole doublet was not observed in the spectrum of iron oxide nanoparticles synthesized without HA (Fig. 11). The HA addition to the solution resulted in the limited growth of nanoparticles and their stabilization as well as in the formation of a new, intermediate phase. For example, a quadrupole doublet with broadened lines was fixed where the HA concentration was 20 % mass.

The HA concentration increase in nanocomposites led to a buildup of the doublet's relative intensity. The Zeeman sextet with the average Mössbauer line shift $\langle \delta \rangle = 0.48$ and $\langle \delta \rangle = 0.25$ corresponded to Fe(III) atom sites octahedrally and tetrahedrally surrounded by oxygen, respectively, and $\langle \delta \rangle = 0.65$—to Fe(II) atoms in the octahedral surrounding of oxygen atoms. Evaluation of particle sizes showed that iron oxide particles were downsized with the HA content increase in the composition of hybrid materials: *d* (Fe_3O_4-HA20-C) = 13.5 ± 0.1 nm and *d* (Fe_3O_4-HA50-C) = 12.3 ± 0.1 nm.

The Mössbauer spectra of hybrid materials attained by the mechanochemical method also represented asymmetric Zeeman sextets with broadened lines, which is characteristic of superparamagnetic particles. The quadrupole doublet with the average parameters $\langle \delta \rangle = 0.36 \pm 0.01$ mm/s and $\langle \varepsilon \rangle = 0.50 \pm 0.04$ mm/s corresponded to Fe(III) sites tetrahedrally surrounded by oxygen atoms in the new phase structure on the surface of hybrid materials [69]. The phase ratio and particle size of magnetite and the Fe_3O_4-HA20-M10 sample did not actually differ whereas the sample with the 20 % mass concentration of HA was largely maghemite (γ-Fe_2O_3).

Fig. 11 Mössbauer spectra of hybrid materials: *1* Fe₃O₄-HA20-C, *2* Fe₃O₄-HA50-C, *3* Fe₃O₄-HA80-C, prepared from magnetite and HA by chemical coprecipitation in argon; recorded at 5s К [69]
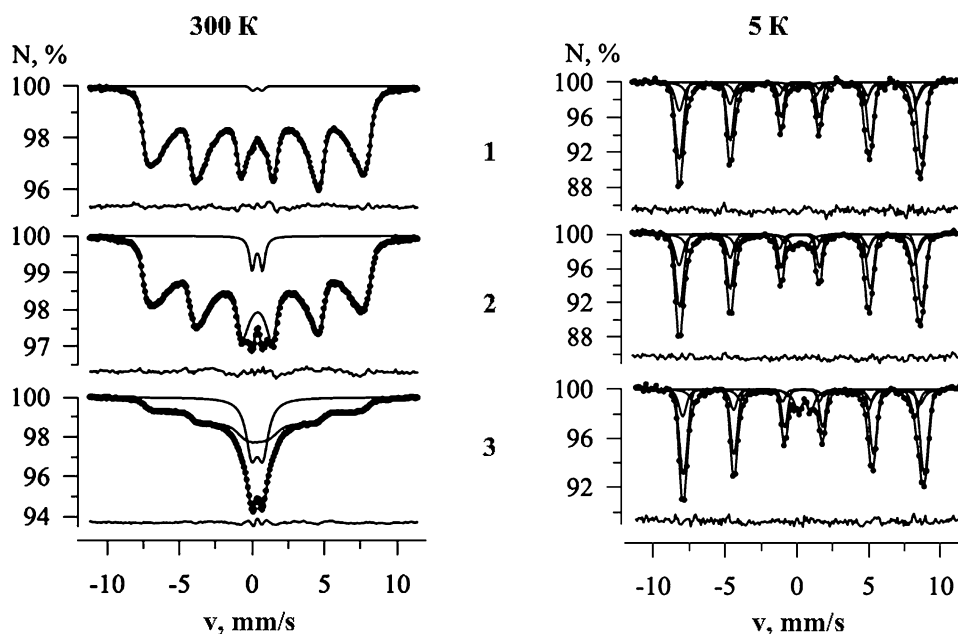
Due to diversity of the functional groups of humic acids, it is very difficult to make a definite conclusion about the mechanism of stabilization and regulation of growth of magnetite nanoparticles in the HA medium. However, it can be naturally assumed that at pH > 9 carboxylic groups are involved in the process of coordination of the magnetite with the HA [120]. It follows from the IR spectroscopy data that the spectra of the materials obtained have intense bands in the 1530–1570 cm^{-1} (C=O), 1360–1370 cm^{-1} (C=O), 400–600 cm^{-1} (Fe–O), and 3400–3000 cm^{-1} (O–H) regions. In addition, the characteristic vibration band of the carbonyl group (vCO = 1640–1740 cm^{-1}) becomes weaker. At the same time, the bands, correspondent to symmetric (v_sCOO = 1390–1400 cm^{-1}) and asymmetric (v_{as}COO = 1560–1590 cm^{-1}) vibrations of carboxylated ions appear in spectra [68].

Interaction of iron (III) ions affects the bands for carbonyl groups: aliphatic (1100 cm^{-1}), aromatic (1300 cm^{-1}), inter alia, those with double conjugated links (1600 cm^{-1}), present in benzene and quinoid compounds in humic acid molecules [68]. The appearance of bonds between iron ions and benzene and quinoid fragments is confirmed by fluorescent analysis data [121]. With complete saturation of such bonds, iron interacts with amino groups (the appearance of peaks in the 2300 and 3000–3400 cm^{-1} regions), making part of the humic acid heterocyclic fragments [68].

Thus, humic acids that represent polyanions in water solutions, being introduced into the system as agents stabilizing the growth of iron oxide nanoparticles, interact electrostatically with positively charged nanoparticles of iron oxide depending on the pH of solution, since both partners in the electrostatic interactions have definitely pH-dependent charge state in aqueous solutions. On the one hand, the dissociation of humic acids results in polyanions indeed from relatively low pH (∼1, since below it, HA precipitates as seen in the isolation scheme of humic substances recommended by [122]). On the other hand, the forming iron oxide nanoparticles have positively charged surface only below its PZC or IEP (pH ∼ 7–8) as discussed in [26, 42, 86, 87].

As seen from the scheme (Fig. 12), a scope of possible complexes of HA with iron oxides is wide and definitely not limited to the above-mentioned component forms and interaction types.

Functional groups of HA were likely to occupy all sites available for the coordination on the surface of nanoparticles, i.e., smaller nanoparticles took on a polyanionic coating and were absorbed by the dendrite-like HA structure.

According to scanning electronic microscopy data, when a magnetite is added to humic acids in the presence of NH₄OH, the compactness and the structure of humic acid macromolecular associates increases (Fig. 13). As a result of interaction between iron ions and active ionogenic groups of humic acid macromolecules the negative charge of individual links decreases, thus leading to a decrease in the energy of their repulsion and, along with direct interaction of active groups via ions, to formation of compact associate complexes, which is typical of polymeric electrolytes [68].

The dissolution method for preparing nanocomposites is based on the in situ chemical coprecipitation technology used to form hydrated ferric oxide (magnetite) from aliovalent iron salts taken in quantitative ratios Fe^{2+}/Fe^{3+} = 1:2 in the alkaline medium and in the presence of a stabilizing polymeric ligand, viz. humic acids. It is the

Fig. 12 Possible schemes of interactions between iron oxides and HA [123, adapted]
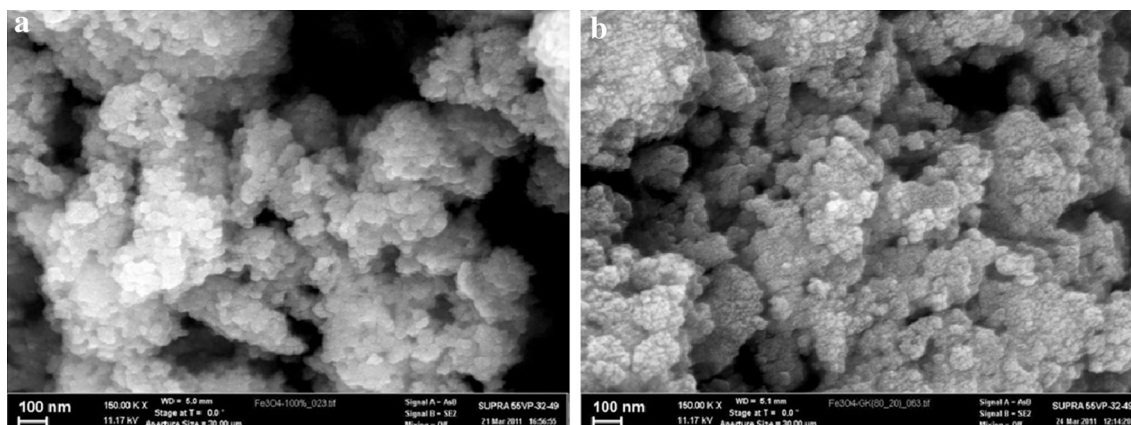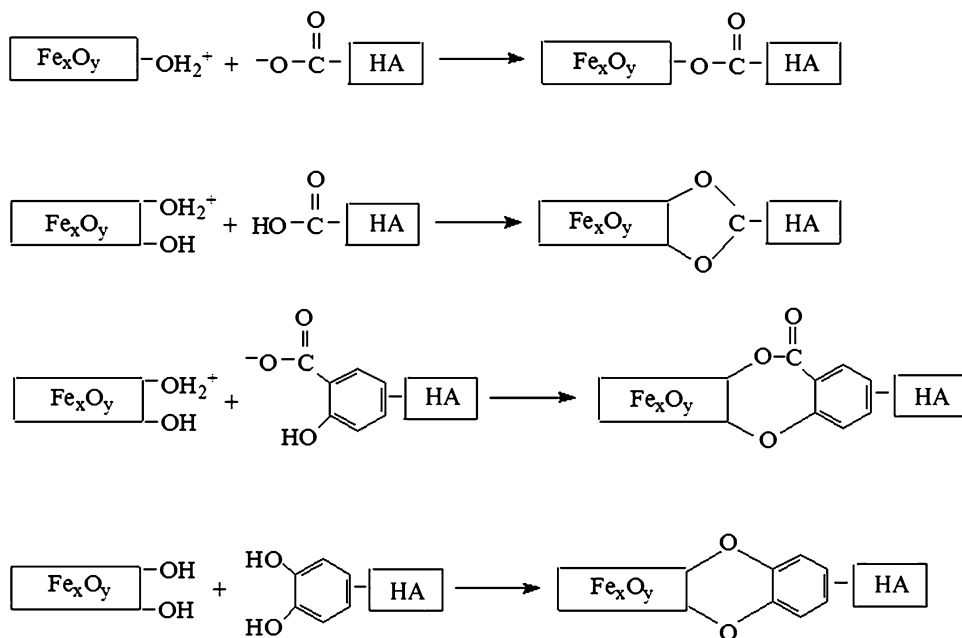

Fig. 13 SEM micrographs: **a** Fe_3O_4; **b** Fe_3O_4-HA20-M10 (index "M10" means mechanochemical dispersion during 10 min)

most optimal method in terms of forecastability, reproducibility and identification of the crucial parameters responsible for control of targeted properties.

The mechanochemical synthesis gives rather contrary results of both decreasing and increasing particle sizes which varied over a wide range from nano- to micrometer dimensions, depending on the synthesis conditions, with the parallel enhancement of their by-size distribution.

6.1 Magnetic Properties of Nanocomposites Based on Magnetite and Humics

An objective in the creation of functional magnetite and HA-based nanomaterials is to gain synergism and control of properties of the polymeric matrix and material of the central nanosized nucleus of iron oxides. This will let

implement magnetic separation approaches that ensure predicted sorption and magnetic properties of starting components. Magnetic properties of nanoparticles are governed by many factors such as the chemical composition, particle size and shape, interaction of particles with the surrounding matrix, etc.

Remagnetization curves for Fe_3O_4, Fe_3O_4-HA20-C, Fe_3O_4-HA50-C, and Fe_3O_4-HA80-C samples at different temperatures are presented in Fig. 14 [69]. The shape of the remagnetization curves was characteristic of ferromagnetics and, at the same time, a change in the parameters of hysteresis loops was observed with a change of the HA concentration in the materials. The hysteresis loop parameters for the Fe_3O_4-HA20-C sample altered insignificantly, as compared to native magnetite; however, where the HA concentration was 50 % and more, the loop

assumed a narrower shape (Fig. 14). A hysteresis loop narrowing was also noted where the remagnetization curves were measured at a higher temperature. This behavior is related to the increase in the energy of thermal vibrations of the magnetic moment of hybrid material particles.

An approximation of experimental points was performed to obtain the hysteresis loop parameters for the test samples. The modified Langevin function was used as a hysteresis model [69]:

$$M = \chi H + M_S(\coth(H - H_C)\chi_{in}) - 1/((H - H_C)\chi_{in}),$$
(10)

where χ—magnetic permeability of a test sample;

M_S—saturation magnetization;

χ_{in}—initial magnetic permeability;

H_c—coercive force.

The coercive force and magnetization saturation determined in this manner were calculated per volume unit (the average density of hybrid materials was assumed as 2 g/cm^3). Additionally, the effective anisotropy constant was evaluated by the formula $K_{eff} = H_c M_s^2$.

An analysis of the loop parameters showed that the coercive force reduced with a temperature rise (Table 5). The HA concentration increase in the composition of hybrid materials up to 50 % did not actually lead to coercivity changing whereas, at the 80 % HA concentration, the coercive force diminished several-fold (Fig. 15) [69].

The magnetic anisotropy constant value declined with the HA concentration increase in the composition of hybrid materials, which was also associated with the decrease of the nanocomposite particle size.

Therefore, as follows from the data of Mössbauer and magnetic measurements, the HA addition led to stabilization of particle sizes. Smaller particles were formed in the case of higher HA concentrations. The nucleus of hybrid

materials was a mixture of nonstoichiometric magnetite and maghemite. A new phase was formed at n (HA) >50 % and the partial spectrum parameters corresponded to Fe^{3+} atoms octahedrally surrounded by oxygen [69].

Nanoclusters of iron oxides stabilized by humic acids exhibit superparamagnetic properties at room temperature. An organic modifier, such as HA, for nanoparticles resolves a few problems. Humic acids have a branched molecular structure that permits embedding of several particles rather than just one. They form a distributed associate whose size matches that of the initial HA globule. This allows stabilization of nanoparticles and water suspensions based on them as well as artificial control over magnetic properties of hybrid materials through varying the ratio of humic acids and the embedded nanoparticles.

6.2 Sorption Properties of Nanocomposites Based on Magnetite and Humic Acids

In general, metal sorption in the presence of organic ligands is enhanced at acidic pH values and decreases at high pH values. Electrostatic enhancement is believed to occur by the reduction of the positive mineral surface charge following the adsorption of negative anions, thus resulting in a more attractive surface for adsorption of cations [124]. A ternary cation–anion-surface complex may bind to the surface by inner-sphere (directly bonded to the surface) or outer-sphere (aqua-ion surrounded by water molecules and thus held to the surface of the sorbent by electrostatic attraction) mechanisms [125, 126].

The sorbents under study are characterized by a high sorption capacity regarding to UO_2^{2+}, Cd^{2+}, Pb^{2+}. Such a behavior can be caused by the formation of rather strong metal complexes with humic acids. This is confirmed by the high value of their stability constants (logβ varies from 5.85 to 11 for complexes of the UO_2^{2+}/HA [127]).

Calculated sorption parameters using sorption isotherms in Langmur linearized coordinates are given in Table 6.

The adsorption of metal ions onto the Fe$_3$O$_4$-HA nanocomposite surface is enhanced in comparison with the free HA (Fig. 16). It is known that adsorption behavior of metal ions by mineral oxides can be greatly changed depending on the experimental conditions (pH, ionic strength, the presence and absence of humic acids) [128, 129].

For the systems studied when the magnetite particles stabilized by macromolecules of HA form the stable colloid dispersion in the wide range of pH [88], the enhanced sorption capacity of the Fe$_3$O$_4$-HA nanocomposite can be account for a high dispersion of nanosized magnetite (S_{spec} for HA and Fe$_3$O$_4$-HA made 42 and 62–180 m^2/g, accordingly).
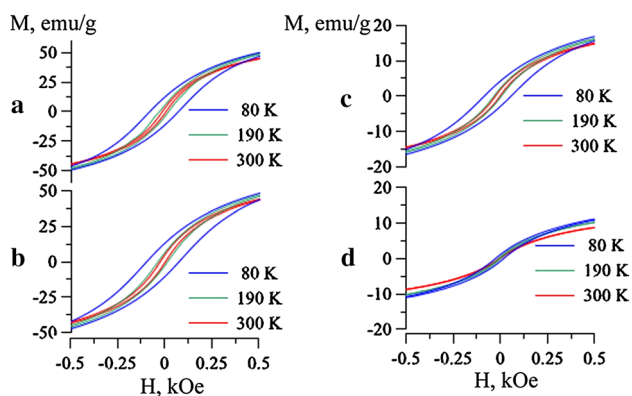
Fig. 14 Magnetic hysteresis loops for hybrid materials Fe$_3$O$_4$ (**a**), Fe$_3$O$_4$-HA20-C (**b**), Fe$_3$O$_4$-HA50-C (**c**), and Fe$_3$O$_4$-HA80-C (**d**) measured at different temperatures [69]

Table 5 Magnetic characteristics of nanocomposites synthesized by chemical coprecipitation with different HA concentrations [69]

HA (%)		0	20	50	80
H_c (Oe)	80 Ќ	65 ± 2	74 ± 2	61 ± 2	20 ± 2
	190 Ќ	20 ± 2	21 ± 2	17 ± 2	6 ± 3
	300 Ќ	9 ± 2	15 ± 2	13 ± 2	3 ± 2
M_s (emu/g)	80 Ќ	75 ± 1	76 ± 1	26 ± 1	17 ± 1
	190 Ќ	71 ± 1	71 ± 1	24 ± 1	16 ± 1
	300 Ќ	65 ± 1	65 ± 1	22 ± 1	14 ± 1
K_{eff} (erg/cm^3)	80 Ќ	2407 ± 69	2811 ± 64	804 ± 20	170 ± 17
	190 Ќ	707 ± 77	747 ± 71	208 ± 22	51 ± 23
	300 Ќ	288 ± 79	497 ± 74	145 ± 22	21 ± 18
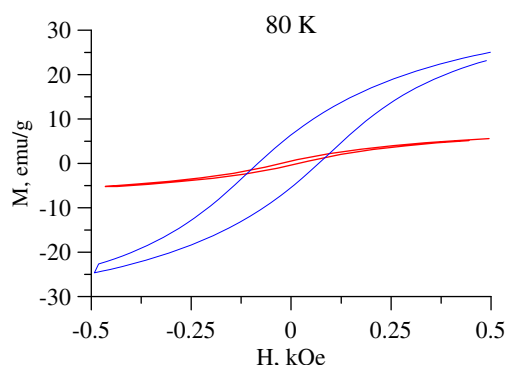
Fig. 15 Magnetic hysteresis loops for *1* Fe$_3$O$_4$ and *2* Fe$_3$O$_4$-HA80-C measured at T = 80 Ќ [69]

Table 6 Calculated sorption parameters for HA and Fe$_3$O$_4$-HA

Sorbent$^+$, M^{2+}	K_{sorp}, 1/M	Q_{max} (mmol/g)
Pb^{2+}/HA	$(4.93 \pm 0.16) \times 10^4$	1.35 ± 0.3
Pb^{2+}/Fe$_3$O$_4$-HA	$(7.8 \pm 0.4) \times 10^4$	1.78 ± 0.2
UO$_2^{2+}$/HA	$(4.1 \pm 1.6) \times 10^4$	0.3 ± 0.05
UO$_2^{2+}$/Fe$_3$O$_4$-HA	$(3.5 \pm 1.4) \times 10^4$	0.56 ± 0.02
Cd^{2+}/HA	580 ± 22	0.82 ± 0.1
Cd^{2+}/Fe$_3$O$_4$-HA	760 ± 12	0.96 ± 0.3

Given that alkaline and alkaline earth metal ions (such as calcium and magnesium) may influence the association of heavy metals with the humic acids. The study [50] was undertaken to estimate the sorption behavior of Fe$_3$O$_4$-HA in the presence of UO$_2^{2+}$ and competition Mg^{2+}.

As shown from the Fig. 17, there was no serious effect on the adsorption of UO$_2^{2+}$ even when the concentration of the coexisting ions was about 100-fold. The competitive adsorption studies showed that the Fe$_3$O$_4$-HA had good adsorption selectivity for UO$_2^{2+}$ with the coexistence of Mg^{2+}.

Thus, it has been established that humic substances, on the one hand, can act as efficient stabilizers for magnetoactive magnetite nanoparticles and let avoid their size
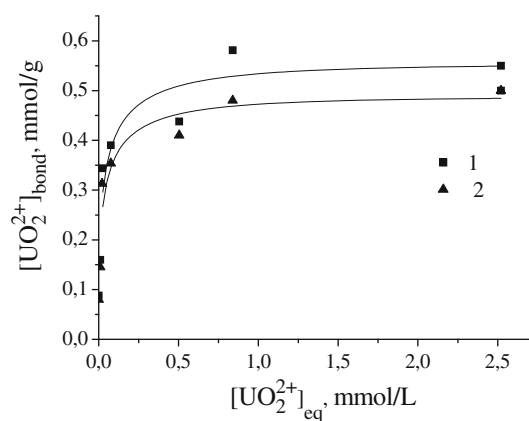

Fig. 16 Adsorption isotherms of UO$_2^{2+}$ onto HA (*1*) and Fe$_3$O$_4$-HA (*2*) nanocomposite

Fig. 17 Adsorption isotherms of UO$_2^{2+}$ onto Fe$_3$O$_4$-HA in the absence (*1*) and in the presence of Mg^{2+} (*2*)

growth, and, on the other hand, they are able to retain the protector properties with respect to ecotoxicants. Developing of materials based on magnetite characteristic of high magnetic performance and humic acids is a promising pathway to hybrid materials for the remediation of disturbed biogeocenoses. Iron mineralization processes, i.e., generation of nanoparticles sorbed (including bonded by primary valence forces) by humic acids in the conditions of

in situ chemical coprecipitaion of magnetite nanoparticles, brings about a capability to form complexes with heavy metals by means of various functional groups with subsequent magnetic separation of the net product and neutralization of toxicants. Furthermore, remediation activities with the use of humic acid derivatives are more cost efficient because HA production is not feedstock-limited and causes less damage to the environment since humic substances are organic products of biocenoses.

7 Conclusion

At present, of high relevance is the development of environmentally safe detoxifying agents with a combined action that would have a high remediation capacity with respect to disturbed biogeocenoses. The application of selective sorbents of inorganic (zeolites) and organic (ion-exchange resins) nature is among the most efficient routes of immobilization of diverse chemical ecotoxicants or radionuclides. However, key demerits of these systems are associated, on the one hand, with a low strength of binding of chemical pollutants, often having the equilibrium nature, and of immobilization of radionuclides and, on the other hand, with difficulties in eliminating (especially in the event of radionuclides) pollutant-sorbent conglomerates and high cost of such sorbents. Existing technologies for the elimination of toxic metal ions such as chemical precipitation, extraction with solvents, ion exchange and membrane techniques, and ultrafiltration have disadvantages such as an incomplete metal removal and high cost due to inter alia great reagent and energy consumption, and, finally, waste disposal processes as such can generate toxic tailings, deposits, etc. Additionally, efficiency and cost aspects gain more topicality where the metal concentration in contaminated environments ranges from 10 to 100 mg/g. Particle elimination from solutions using magnetic fields is a more selective and efficient (and often faster) procedure than centrifuging or filtration. In this context, it seems preferable to utilize magnetoactive materials able to exhibit high performance in the magnetic separation.

A significant, yet so far understudied, benefit is anticipated from organomineral composites that include natural complexons—humic acids exerting high affinity to ions of heavy metals and iron oxides, in particular magnetite. A higher sorption capacity and heavy metal elimination rate can be achieved through the nanomaterial structure control and surface area increase. Humic acids are polyfunctional high-molecular substances of a natural origin with the branched molecular structure and multiple reactive moieties such as carboxylic, phenolic, etc. The potentiality of HA and their derivatives as sorbents in various applications is underpinned by huge humus-containing resources, e.g., brown coal, peat, sapropel, etc. Such hybrid materials have complementary qualities of high performance sorbents and specific magnetic materials. These can underlie a special HA application related to the removal of a magnetoactive pollutant-sorbent conglomerate from contaminated environments by a magnetic separation technique. Due to the fact that the fabrication and further use of a hybrid material as a sorbent are implemented in a few steps, as well as that the duration, energy consumption, and reagents' assortment and amounts directly tell on key performance indicators of the overall process, let alone end product cost and properties, there is a strong need for a search of scientifically grounded approaches focused on end product and technology cost reduction.

References

1. S.P. Gubin, Yu.A Koksharov, G.B. Khomutov, GYu. Yurkov, Russ. Chem. Rev. **74**(6), 489 (2005)
2. D. Duchêne, R. Gref, Int. J. Pharm. **502**, 1 (2016)
3. L.L. Vatta, R.D. Sanderson, K.R. Kokh, Pure Appl. Chem. **78**, 9 (2006)
4. J.-F. Liu, Z-Sh Zhao, G.B. Jiang, Environ. Sci. Technol. **42**, 18 (2008)
5. L-Sh Zhong, J.-S. Hu, H.-P. Liang, A.-M. Cao, W.-G. Song, L.-J. Wan, Adv. Mater. **18**, 18 (2006)
6. M. Kokate, K. Garadkar, A. Gole, J. Mater. Chem. A. **1**, 2022 (2013)
7. Z. Cheng, A.L.K. Tan, Y. Tao, D. Shan, K.E. Ting, X.J. Yin, Int. J. Photoenergy (2012). doi:10.1155/2012/608298
8. L. Carlos, F.S. Garcia Einschlag, M.C. Gonzales, D.O. Martire, in *Waste Water—Treatment Technologies and Recent Analytical Developments*, ed. by F.S. Garcia Einschlag (InTech, Croatia, 2013), pp. 63–77
9. F. Huber, D. Schild, T. Vitova, J. Rothe, R. Kirsch, T. Schäfer, Geochim. Cosmochim. Acta **96**, 154 (2012)
10. Ya. Gong, L. Wang, J. Liu, J. Tang, D. Zhao, Sci. Total Environ. **562**, 191 (2016)
11. Yo. Li, R. Zhang, X. Tian, Ch. Yang, Zh. Zhou, Appl. Surf. Sci. **369**, 11 (2016)
12. Sh. Rajput, Ch.U. Pittman, D. Mohan, J. Colloid Interface Sci. **468**, 334 (2016)
13. Z.F. Akl, Sh.M. El-Saeed, A.M. Atta, J. Ind. Eng. Chem. **34**, 105 (2016)
14. Sh. Yu, L. Zhai, Sh. Zhong, Yo. Qiu, L. Cheng, X. Ren, J. Taiwan Inst. Chem. E. **59**, 221 (2016)
15. A. Mirabi, A.Sh. Rad, S. Nourani, TrAC-Trend. Anal. Chem. **74**, 146 (2015)
16. A.D. Pomogailo, V.N. Kestelman, *Metallopolymer Nanocomposites* (Springer, Heidelberg, 2005), pp. 65–472
17. R.A. Bini, R.F.C. Marques, F.J. Santos, J.A. Chaker, M. Jafelicci Jr., J. Magn. Magn. Mater. **324**, 4 (2012)

18. A.Yu. Gervald, I.A. Gritskova, N.I. Prokopov, Russ. Chem. Rev. **79**(3), 219 (2010)

19. D. Ortega, in *Magnetic Nanoparticles. From Fabrication to Clinical Applications*, ed. by N.T.K. Thanh (CRC Press, Boca Raton, 2012), pp. 3–46

20. M.M. Rahman, Sh.B Khan, A. Jamal, M. Faisal, A.M. Aisiri, in *Nanomaterials*, ed. by M.M. Rahman (InTech, Croatia, 2011), pp. 43–56

21. M. Faraji, Y. Yamini, M. Rezaee, J. Iran. Chem. Soc. **7**, 1 (2010)

22. E. Umut, in *Modern Surface Engineering Treatment*, ed. by M. Aliofkhazraei (InTech, Croatia, 2013), pp. 185–208

23. Y.-W. Jun, J.-W. Seo, J. Cheon, Acc. Chem. Res. **41**, 2 (2008)

24. A. Noori, K. Parivar, M. Modaresi, M. Messripour, M.H. Yousefi, G.R. Amiri, Afr. J. Biotechnol. **10**(7), 1221 (2011)

25. L. Pauling, *General Chemistry* (W.H. Freeman, San Francisco, 1970), pp. 928–938

26. R.M. Cornell, U. Schwertmann, *The Iron Oxides. Structure, Properties, Reactions, Occurrences and Uses* (Wiley VCH Verlag GmbH, Weinheim, 2003), p. 338

27. C. Sun, J.S. Lee, M. Zhang, Adv. Drug Deliver. Rev. **60**(11), 1252 (2008)

28. U. Meisen, H. Kathrein, J. Imaging Sci. Techn. **44**, 508 (2000)

29. Yu.P Grabovsky, *Physico-Chemical Bases of Magnetic Fluids Synthesis* (Stavropol, SGU, 1998), p. 27. **In Russian**

30. D. Högemann, L. Josephson, R. Weissleder, J.P. Basilion, Bioconjugate Chem. **11**, 6 (2000)

31. K. Nishio, M. Ikeda, N. Gokon, S. Tsubouchi, H. Narimatsu, Y. Mochizuki, S. Sakamoto, A. Sandhu, M. Abe, H. Handa, J. Magn. Magn. Mater. **310**, 2408 (2007)

32. D.D. Suppiah, Sh.B.A. Hamid, J. Magn. Magn. Mater. **414**, 204 (2016)

33. J. Sato, M. Kobayashi, H. Kato, T. Miyazaki, M. Kakihana, J. Asian Ceram. Soc. **2**, 3 (2014)

34. A. Sutka, S. Lagzdina, I. Juhnevica, D. Jakovlevs, M. Maiorov, Ceram. Int. **40**, 7 (2014)

35. A.V. Lisin, Yu.P. Grabovsky, Patent RF 2422932 MPK H01F 1/28, C01G49/08. Issue Date 27 June 2011 **In Russian**

36. .S. Papell, Patent US 3215572A H01F 1/44. Issue Date 02 November 1965

37. A. Khataee, M. Taseidifar, S. Khorram, M. Sheydaei, S.W. Joo, J. Taiwan Inst. Chem. Eng. **53**, 132 (2015)

38. H. Setyawan, F. Fajaroh, W. Widiyastuti, S. Winardi, I. Wuled Lenggoro, N. Mufti, J. Nanopart. Res. **14**, 807 (2012)

39. V.M. Makarov, N.N. Bazhanov, M.A. Shipilin, A.M. Shipilin, A.G. Erekhinskaya, S.Z. Kalaeva, I.N. Zakharova, Patent RF 2363064 MPK H01F 1/28. Issue Date 27 July 2009 **In Russian**

40. R. Kumar, R. Sakthivel, R. Behura, B.K. Mishra, D. Das, J. Alloy Compd. **645**, 398 (2015)

41. E. Amstad, S. Zurcher, A. Mashaghi, J.Y. Wong, M. Textor, E. Reimhult, Small **5**, 11 (2009)

42. E. Tombacz, A. Majzik, Z. Horvat, E. Illes, Rom. Rep. Phys. **58**, 3 (2006)

43. E. Tombacz, I.Y. Toth, D. Nesztor, E. Illes, Colloid Surf. A **435**, 91 (2013)

44. A. Aqil, S. Vasseur, E. Duguet, C. Passirani, J.P. Benoit, A. Roch, R. Muller, R. Jerome, C. Jerome, Eur. Polym. J. **44**, 10 (2008)

45. T. Sen, S.J. Sheppard, T. Mercer, M. Eizadi-Sharifabad, M. Mahmoudi, A. Elhissi, RSC Adv. **2**, 5221 (2012)

46. Y. Zhang, C. Sun, N. Kohler, M. Zhang, Biomed. Microdevices **6**(1), 33 (2004)

47. W.C. Elmore, Phys. Rev. B **54**, 1092 (1938)

48. Y.-H. Deng, C.-C. Wang, J.-H. Hu, W.-L. Yang, Sh-K Fu, Colloid Surf. A **262**, 87 (2005)

49. R.A. Ali-Zade, Turk. J. Phys. **28**, 359 (2004)

50. A.D. Pomogailo, K.A. Kydralieva, A.A. Zaripova, V.S. Muratov, G.I. Dzhardimalieva, S.I. Pomogailo, N.D. Golubeva, Sh.J. Jorobekova, Macromol. Symp. **304**, 18 (2011)

51. J.H. Kwon, L.D. Wilson, R. Sammynaiken, Synth. Met. **197**, 8 (2014)

52. K.Y. Yoon, Z. Xue, Y. Fei, J.H. Lee, V. Cheng, H.G. Bagaria, C. Huh, S.L. Bryant, S.D. Kong, V.W. Ngo, A.-R. Rahmani, M. Ahmadian, C.J. Ellison, K.P. Johnston, J. Colloid Interface Sci. **462**, 359 (2016)

53. Z. Li, Q. Sun, M. Gao, Angew. Chem. Int. Edit. **44**, 123 (2005)

54. P. Granitzer, K. Rumpf, Materials **4**, 908 (2011)

55. L.A. Bondar, N.V. Abramov, V.N. Mishchenko, P.P. Gorbik, Colloid J. **72**, 1 (2010)

56. Y. Tan, Zh. Zhuang, Q. Peng, Ya. Li, Chem. Mater. **20**, 5029 (2008)

57. M. Ghazanfari, A. Yazdani, Mat. Sci. Semicond. Proc. **40**, 152 (2015)

58. T. Iwamoto, T. Kinoshita, K. Takahashi, J. Solid State Chem. **237**, 19 (2016)

59. X. Shi, S.H. Wang, S.D. Swanson, S. Ge, Z. Cao, M.E. Van Antwerp, K.J. Landmark, J.R. Baker, Adv. Mater. **20**, 9 (2008)

60. C.J. Xu, S.H. Sun, Polym. Int. **56**, 821 (2007)

61. L. Babes, B. Denizot, G. Tanguy, J.J. Le Jeune, P. Jallet, J. Colloid Interface Sci. **212**, 474 (1999)

62. H.-C. Roth, S.P. Schwaminger, M. Schindler, F.E. Wagner, S. Berensmeier, J. Magn. Magn. Mater. **377**, 81 (2015)

63. F. Dang, N. Enomoto, J. Hojo, K. Enpuku, J. Cryst. Growth **312**, 10 (2010)

64. M. Jean, V. Nachbaur, J.-M. Le Breton, J. Alloy Compd. **513**, 154 (2012)

65. I.V. Aleksashkin, K.D. Pershina, K.A. Kazdobin, Scientific notes of Taurida V. Vernadsky National University. Series: biology, chemistry. **23**, 3 (2010) **In Russian**

66. A.Yu. Gervald, N.I. Prokopov, Yu.M. Shiryakina, Vestnik MITHT. **5**, 3 (2010) **In Russian**

67. A. Yurishcheva, G.I. Dzhardimalieva, S. Pomogailo, A.D. Pomogailo, Sh Jorobekova, K. Kydralieva, Macromol. Symp. **317–318**(1), 169 (2012)

68. A.A. Yurishcheva, G.I. Dzhardimalieva, E.J. Kasymova, S.I. Pomogailo, K.A. Kydralieva, S.P. Li, Nanomech. Sci. Technol: Int. J. **5**(4), 323 (2014)

69. N.I. Chistyakova, A.A. Shapkin, T.V. Gubaidulina, M.E. Matsnev, R.R. Sirazhdinov, A.P. Kazakov, V.S. Rusakov, Hyperfine Interact. **226**, 1–3 (2014)

70. V.V. Boldyrev, Russ. Chem. Rev. **75**(3), 177 (2006)

71. T. Iwasaki, N. Sato, H. Nakamura, S. Watano, Adv. Powder Technol. **24**, 2 (2013)

72. T. Iwasaki, N. Sato, H. Nakamura, S. Watano, Mater. Chem. Phys. **140**, 2–3 (2013)

73. C.-R. Lin, Y.-M. Chu, S.-C. Wang, Mater. Lett. **60**, 4 (2006)

74. S.J. Campbell, W.A. Kaczmarek, G.-M. Wang, Nanostruct. Mater. **6**, 5–8 (1995)

75. F. Orru, *Design of Functional Colloidal Magnetic Nanoparticles for Biomedical Applications* (Università degli Studi di Cagliari, 2012)

76. R.L. Rebodos, P.J. Vikesland, Langmuir. **26**(22), 16745 (2010)

77. E. Tombácz, R. Turcu, V. Socoliuc, L. Vékás, Biochem. Biophys. Res. Commun. **468**, 442 (2015)

78. S. Laurent, A.A. Saei, S. Behzadi, A. Panahifar, M. Mahmoudi, Expert Opin. Drug Deliv. **11**, 1449 (2014)

79. A.D. Pomogailo, G.I. Dzhardimalieva, V.N. Kestelman, *Macromolecular Metal Carboxylates and Their Nanocomposites* (Springer, Berlin, 2010), p. 182

80. Y. Sun, L. Duan, Z. Guo, Y. DuanMu, M. Ma, L. Xu, Y. Zhang, N. Gu, J. Magn. Magn. Mater. **285**, 65 (2005)

81. J. Lee, Y. Lee, J.K. Youn, H.B. Na, T. Yu, H. Kim, S.M. Lee, Y.M. Koo, J.H. Kwak, H.G. Park, H.N. Chang, M. Hwang, J.G. Park, J. Kim, T. Hyeon, Small **4**, 1 (2008)

82. F. Fajaroh, H. Setyawan, A. Nur, I.W. Lenggoro, Adv. Powder Technol. **24**, 2 (2013)

83. A.H. Lu, E.L. Salabas, F. Schuth, Angew. Chem. Int. Edit. **46**, 1222 (2007)

84. N. Zakharova, K. Kydralieva, E. Khudaibergenova, N. Gorbunova, S. Pomogailo, G.I. Dzhardimalieva, A. Pomogailo, Sh Jorobekova, Macromol. Symp. **317–318**, 1 (2012)

85. T.A. Sorkina, A.Yu. Polyakov, N.A. Kulikova, A.E. Goldt, O.I. Philippova, A.A. Aseeva, A.A. Veligzhanin, Y.V. Zubavichus, D.A. Pankratov, E.A. Goodilin, I.V. Perminova, J. Soil Sediment. **14**, 2 (2014)

86. M. Szekeres, I.Y. Tóth, E. Illés, A. Hajdu, I. Zupko, K. Farkas, G. Oszlanczi, L. Tiszlavicz, E. Tombacz, Int. J. Mol. Sci. **14**, 14550 (2013)

87. E. Illes, E. Tombacz, Colloids Surf. A **230**, 99 (2003)

88. E. Illes, E. Tombacz, J. Colloid Interface Sci. **295**, 115 (2006)

89. C.T. Yavuz, J.T. Mayo, W.W. Yu, A. Prakash, J.C. Falkner, S. Yean, L. Cong, H.J. Shipley, A. Kan, M. Tomson, D. Natelson, V.L. Colvin, Science. **314**, 964 (2006)

90. S. Wei, Y. Zhang, J. Xu, Colloid Surface A **296**, 1–3 (2007)

91. J.J. Yuan, S.P. Armes, Y. Takabayashi, K. Prassides, C.A.P. Leite, F. Galembeck, A.L. Lewis, Langmuir. **22**(26), 10989 (2006)

92. J. Lee, T. Isobe, M. Senna, J. Colloid Interface Sci. **177**, 490 (1996)

93. P. Gong, J. Yu, H. Sun, J. Hong, S. Zhao, D. Xu, S. Yao, J. Appl. Polym. Sci. **101**, 3 (2006)

94. M. Szekeres, E. Illés, C. Janko, K. Farkas, I.Y. Tóth, D. Nesztor, I. Zupkó, I. Földesi, C. Alexiou, E. Tombácz, Nanomed. Nanotechnol. **5**, 6 (2015)

95. J.S. Salazar, L. Perez, O. De Abril, L.T. Phuoc, D. Ihiawakrim, M. Vazquez, J.-M. Greneche, S. Begin-Colin, G. Pourroy, Chem. Mater. **23**, 1379 (2011)

96. A.G. Roca, J.F. Marco, M.P. Morales, C.J. Serna, J. Phys. Chem. C. **111**(50), 18577 (2007)

97. A.G. Roca, D. Niznansky, J. Poltierova-Vejpravova, B. Bittova, M.A. Gonzalez-Frenandez, C.J. Serna, M.P. Morales, J. Appl. Phys. **105**, 114309 (2009)

98. M.A. Ramazanov, R.A. Ali-zade, P.B. Agakishieva, Dig. J. Nanomater. Biostruct. **5**, 3 (2010)

99. A.-F. Ngomsik, A. Bee, M. Draye, G. Cote, V. Cabuil, CR Chim. **8**, 963 (2005)

100. J. Hu, M.C. Lo, G.H. Chen, Water Sci. Technol. **50**, 139 (2004)

101. Y.-C. Chang, D.-H. Chen, J. Colloid Interface Sci. **283**, 446 (2005)

102. W. Yantasee, C.L. Warner, T. Sangvanich, R.S. Addleman, T.G. Carter, R.J. Wiacek, G.E. Fryxell, C. Timchalk, M.G. Warner, Environ. Sci. Technol. **41**, 5114 (2007)

103. D. Maity, D.C. Agrawal, J. Magn. Magn. Mater. **308**, 46 (2007)

104. A. Tayyebi, M. Outokesh, Sh. Moradi, A. Doram, Appl. Surf. Sci. **353**, 350 (2015)

105. M. Kumari, Ch.U Pittman, D. Mohan, J. Colloid Interface Sci. **442**, 120 (2015)

106. S. Nethaji, A. Sivasamy, A.B. Mandal, Bioresour. Technol. **134**, 94 (2013)

107. S. Venkateswarlu, S.H. Kumar, N.V.V. Jyothi, Water Resour. Ind. **12**, 1 (2015)

108. M. Faraji, Y. Yamini, E. Tahmasebi, A. Saleh, F. Nourmohammadian, J. Iran. Chem. Soc. **7**, 2 (2010)

109. B.S. Inbaraj, B.H. Chen, Bioresour. Technol. **102**, 19 (2011)

110. D.S. Orlov, *Soil Humic Acids and General Theory of Humification* (Moscow, MSU, 1990), p. 325. **In Russian**

111. E.M. Thurman, *Organic Geochemistry of Natural Waters* (Springer, Netherlands, 1985), p. 497

112. D. Kleinhempel, Albrecht-Thaer-Archiv. **14**, 3 (1970)

113. D.S. Orlov, *Humic Substances in Biosphere* (Nauka, Moscow, 1993), pp. 16–27. **In Russian**

114. G.M. Varshal, T.K. Velikhanova, N.M. Baranova, Geochemistry. **3**, 316 (1990)

115. A. Dabrowski, Z. Hubicki, P. Podkocielny, E. Robens, Chemosphere. **56**, 91 (2004)

116. ShJ Jorobekova, *Macroligand Properties of Humic Acids* (Frunze, Ilim, 1987), p. 196. **In Russian**

117. I.V. Perminova, *Analysis, Classification and Predictive Modelling of Properties of Humic Substances* (Moscow, MSU, 2000), p. 359. **In Russian**

118. M. Szylak-Szydlowski, Ecol. Chem. Eng. S. **19**, 405 (2011)

119. T. Jin, X. Zhang, J. Xu, Chinese. J. Appl. Chem. **33**, 3 (2016)

120. P.G. Casillas, C.R. Gonsalez, C.M. Perez, in *Infrared Spectroscopy—Material Science, Engineering and Technology*, ed. by T. Theophile (InTech, Croatia, 2012), pp. 405–420

121. S. Burikov, T. Dolenko, N. Gorbunova, O. Gosteva, D. Khundzhua, K. Kydralieva, S. Patsaeva, V. Yuzhakov, A. Yurischeva, in *Functions of Natural Organic Matter Changing Environment*, ed. by J. Xu, J. Wu, Y. He (Zhejiang University Press, Springer, Dordrecht, 2013), pp. 799–804

122. R.S. Swift, Isolation of IHSS soil fulvic and humic acids (Soil Science Society of America, 1996), http://www.humicsubstances.org/soilhafa.html. Accessed 26 May 2016

123. B. Gu, J. Schmitt, Z. Chen, L. Liang, J.F. McCarthy, Environ. Sci. Technol. **28**, 38 (1994)

124. C. Gessa, M.L. De Cherchi, P. Melis, G. Micera, L.S. Erre, Colloid Surf. **11**, 109 (1984)

125. M.M. Benjamin, J.O. Leckie, Environ. Sci. Technol. **15**, 1050 (1981)

126. J.A. Davis, J.O. Leckie, Environ. Sci. Technol. **12**, 1309 (1978)

127. G.R. Choppin, *Chemical Separation Technologies and Related Methods of Nuclear Waste Management* (Kluwer Academic Publishers, Dordrecht, 1999), pp. 247–260

128. C. Hsi, D. Langmuir, Geochim. Cosmochim. Acta. **45**, 1931 (1985)

129. T. Missana, M. Garcia-Gutierrez, C. Maffiotte, J. Colloid Interface Sci. **260**, 291 (2003)